

Origami/Kirigami-Guided Morphing of Composite Sheets

Jianxun Cui, Felipe R. Pobleto, and Yong Zhu*

Several strategies are recently exploited to transform 2D sheets into desired 3D structures. For example, soft materials can be morphed into 3D continuously curved structures by inducing nonhomogeneous strain. On the other hand, rigid materials can be folded, often by origami/kirigami-inspired approaches (i.e., flat sheets are folded along pre-designed crease patterns). Here, for the first time, combining the two strategies, composite sheets are fabricated by embedding rigid origami/kirigami skeleton with creases into heat shrinkable polymer sheets to create novel 3D structures. Upon heating, shrinkage of the polymer sheets is constrained by the origami/kirigami patterns, giving rise to laterally nonuniform strain. As a result, Gaussian curvature of the composite sheets is changed, and flat sheets are transformed into 3D curved structures. A series of 3D structures are folded using this approach, including cones and truncated pyramids with different base shapes. Flat origami loops are folded into step structures. Tessellation of origami loops is transformed into 3D checkerboard pattern.

The third strategy is to create laterally nonuniform strain, which can change the Gaussian curvature of the sheet (i.e., shape morphing).^[12] A flat sheet (zero Gaussian curvature) can be morphed into a spherical (positive Gaussian curvature) or saddle (negative Gaussian curvature) surface. As an example, hydrogel is widely used for this purpose, as it undergoes large swelling that can be modulated by concentration,^[12c] crosslinking density^[2a,13] and temperature,^[6a] and nonuniform swelling can be achieved by varying these parameters laterally.

In addition to the abovementioned actuation strategies, geometrical design is critical for assembling 2D sheets into desired 3D structures.^[14] A promising design strategy is inspired by origami, an ancient art of paper folding. The crease patterns for desired 3D shapes have been proposed.^[15] However, origami deals with


1. Introduction

Transforming 2D sheets into 3D objects is an emerging topic with many applications, including reconfigurable devices,^[1] self-folding robotics,^[2] smart textiles,^[3] and containers for drug delivery.^[4] Several strategies have been developed to actuate the transformation.^[5] In the first strategy, a 2D sheet is bent into a 3D structure due to varying strain across the thickness.^[6] The varying strain can be induced by unsymmetrical heating^[7] or swelling^[8] in a monolayer sheet of responsive materials, or more commonly, by mismatch strain in a bilayer sheet.^[6a,9] Depending on the strain anisotropy in the two layers, the bilayer sheet can be bent into a cylindrical, spherical, or saddle surface.^[6b] Of note is that the spherical or saddle surface is stable only at small mismatch strain and tends to switch to the cylindrical surface at large mismatch strain.^[10] In the second strategy, 3D structures are assembled from 2D precursors through controlled compressive buckling.^[1b,11] In this case, the 2D precursors do not need to be responsive, as buckling is triggered by external actuators.

intact and nonstretchable sheets, thus it can only generate surfaces with zero Gaussian curvature.^[16] To overcome this limitation and realize nonzero Gaussian curvatures, slits and perforations can be introduced to the 2D sheets prior to folding, which is known as kirigami.^[17] In previous studies, origami/kirigami structures were typically folded via the first or second actuation strategy.^[18]

Here, we report a new approach for shape morphing of 2D composite sheets guided by origami/kirigami design rules and induced by laterally nonuniform strain. A heat shrinkable polymer sheet is used as the actuating material. The origami/kirigami patterns are created by bonding paperboard panels on selected areas of the polymer sheet, which leads to nonuniform lateral shrinkage of the polymer sheet upon heating. The laterally nonuniform strain can in turn change the Gaussian curvature. In the first configuration, an angular shrinkage gadget is created by constraining two radii of a circular polymer sector, resulting in an angular defect (positive Gaussian curvature) around a vertex, which is harnessed to fold origami structures. A single gadget is used to fold a single crease, while multiple gadgets are used to fold multiple creases in a parallel manner. In the second configuration, a minimal surface gadget is created by constraining all the edges of a quadrilateral polymer sheet, which transforms the polymer sheet into a saddle surface (negative Gaussian curvature). The minimal surface gadget is then harnessed to fold flat origami loops into step structures. Finally, 2D tessellation of the origami loops is transformed into a 3D checkerboard pattern.

Dr. J. Cui, F. R. Pobleto, Prof. Y. Zhu
Department of Mechanical and Aerospace Engineering
North Carolina State University
Raleigh, NC 27695, USA
E-mail: yong_zhu@ncsu.edu

 The ORCID identification number(s) for the author(s) of this article can be found under <https://doi.org/10.1002/adfm.201802768>.

DOI: 10.1002/adfm.201802768

2. Results and Discussion

2.1. Folding Using Angular Shrinkage Gadget

Without constraint, the polystyrene (PS) sheet shrinks equiaxially upon heating above the glass transition temperature ($\approx 150^\circ\text{C}$), undergoing a similarity transformation, i.e., the size is reduced while the shape is preserved. The sheet remains flat (zero Gaussian curvature) after shrinking. With constraint, the uniform shrinkage is distorted. **Figure 1** shows a case when two radii of a PS sector were constrained by two rigid bars. The two radii cannot shrink or bend but can rotate. The PS sector still tended to shrink upon heating. As a result, two rigid bars rotated toward each other to reduce the bounding area. The (central) angle of the sector shrank upon heating, resulting in an angular shrinkage gadget.

Sectors of different initial angles were studied. **Figure 1A** shows the optical images before and after shrinking. **Figure 1B**

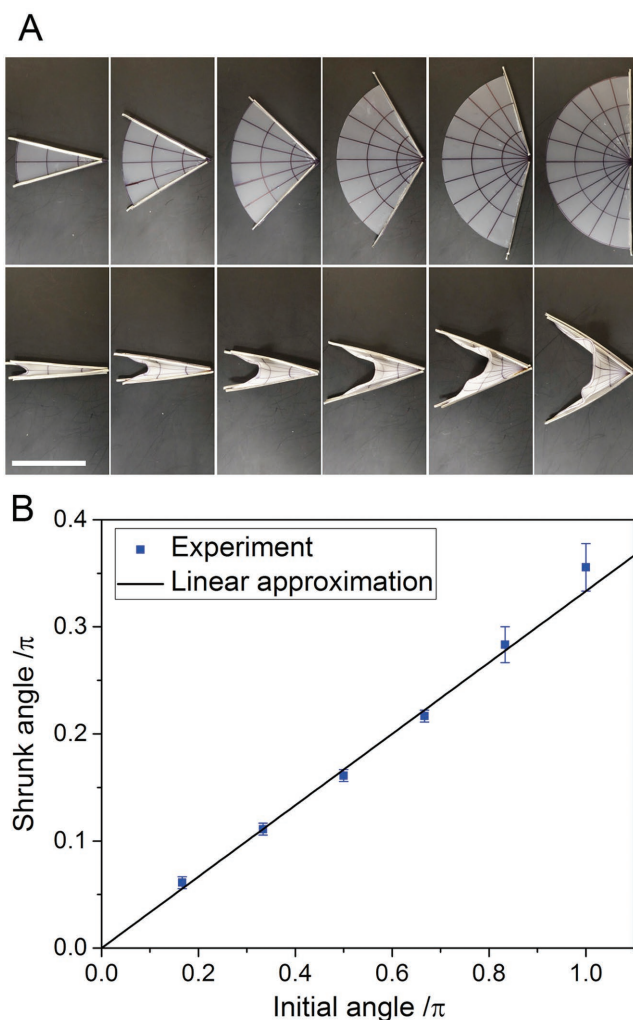


Figure 1. Angular shrinkage gadget. A) Images showing the angular shrinkage with different initial angles. Top: before shrinking; bottom: after shrinking. Scale bar: 30 mm. B) Plot of the shrunk angle as a function of the initial angle. A linear approximation ($y = x/3$) is included for comparison.

shows the shrunk angle as a function of the initial angle. Approximately, shrunk angle increased linearly with the initial angle with the slope of $1/3$. This relationship will be used as a guideline in designing the following structures. The simulated shrunk angles using finite element analysis (FEA) were shown in **Figure S1** in the Supporting Information, in good agreement with the experimental results. In addition, the flat PS sheet was morphed into a saddle surface (**Figure S2**, Supporting Information), which is a minimal surface (with minimal surface area for given boundary conditions).^[12a] It is of interest to note the factor of $1/3$ between the shrunk angle and the initial angle. The factor of $1/3$ is empirical and approximate according to our experimental observations and difficult to quantify analytically. Indeed this factor depends on the biaxial strain in the prestrained PS sheet.

Next, this angular shrinkage gadget was utilized to create angular defect and change the Gaussian curvature of a flat sheet. Note that on a flat surface, which has zero Gaussian curvature everywhere, the angle around a point is 2π . If a sector is cut out of a circular disk and the exposing edges are joined together, a cone can be obtained. It has an angular defect and a positive Gaussian curvature on the vertex. Moreover, the lateral surface is uniformly curved since the stiffness is uniform. In this work, instead of removing a sector, the angular defect was generated by shrinking a sector. In addition, the curving deformation was localized at predefined creases following the origami approach. Note that in folded origami structures (e.g., polyhedrons) with sharp edges and vertices, Gaussian curvature is defined as angular defect around the vertices.^[19]

Figure 2 shows folding of a single crease using an angular shrinkage gadget. **Figure 2A** shows the schematic representation of the folding. The initial state is a flat composite sheet, composed of three sectors: two paperboard sectors (in red) and one PS sector (in blue). For each paperboard sector, two paperboard panels are glued on both sides of the PS sheet. The two paperboard sectors are hinged with a soft crease that is free to rotate. The Gaussian curvature is zero for this flat sheet. In the flat state, the structure can be fully characterized by two independent parameters: angle β of one paperboard sector and angle α of the PS sector. Angle of the other paperboard sector can be calculated by subtracting α and β from 2π . Upon heating, the PS sector shrinks its angle and generates an angular defect (defined as 2π minus the sum of total angles around a vertex). A cone is then formed, which is accompanied by folding of the paperboard sectors along the crease. There exists a relationship between the angular defect and the folding angle, which is defined as the dihedral angle (θ) between the two paperboard sectors. When the PS sector angle shrinks to $\alpha/3$ (corresponding to an angular defect of $2\alpha/3$), it folds the paperboard sectors to a certain dihedral angle(θ). This can be solved via spherical trigonometry,^[16a] as shown in **Figure 2A**. The structure is drawn in a sphere of unit radius. The sector angle is equal to the arc length of a big circle on the surface of the sphere, while the dihedral angle is equal to the angle formed by arcs on the surface of the sphere. The dihedral angle(θ) and the three sector angles ($\alpha/3$, $\alpha + \beta - \pi$, $\pi - \beta$) are related by spherical law of cosines

$$\cos(\alpha/3) = \cos(\alpha + \beta - \pi)\cos(\pi - \beta) + \sin(\alpha + \beta - \pi)\sin(\pi - \beta)\cos(\theta) \quad (1)$$

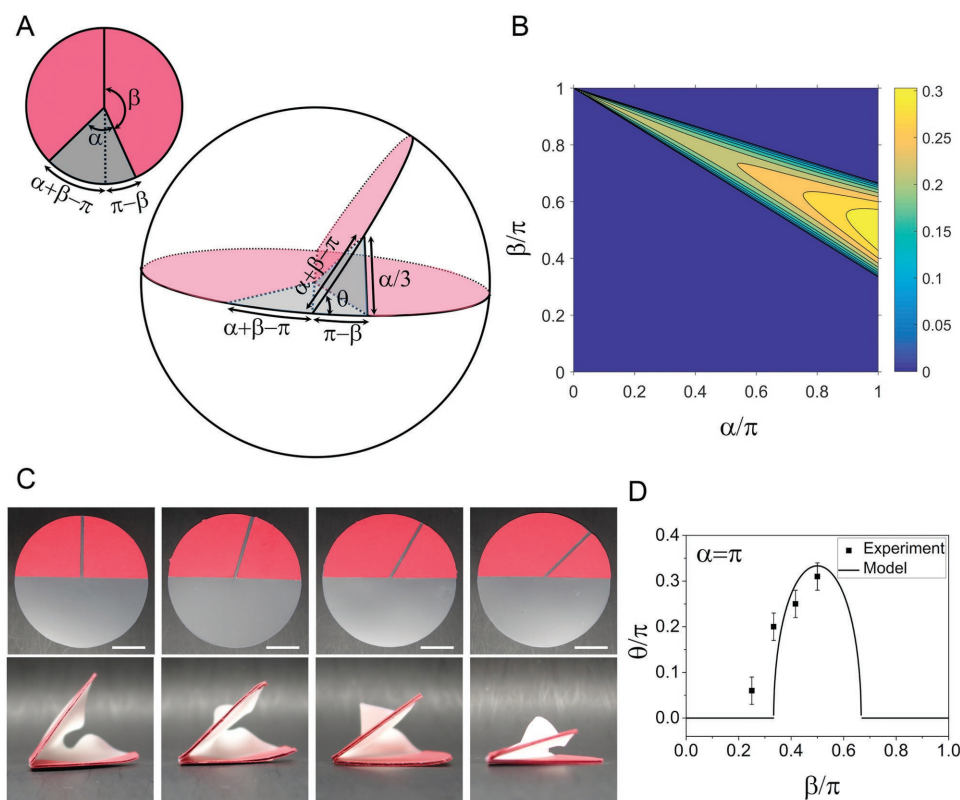


Figure 2. Folding of a single crease using a single angular shrinkage gadget. A) Schematic representation of the folding and related parameters. Red: paperboard sector; blue: PS sector. B) Contour plot of the dihedral angle (θ) as a function of the sector angles (α, β). C) Images showing the folding of a single crease with fixed α ($\alpha = \pi$) and varying β . Top: before folding; bottom: after folding (side view). Scale bars: 30 mm. D) Plot of θ as a function of β ($\alpha = \pi$).

The dihedral angle (θ) can be obtained by solving this equation. Figure 2B shows the contour plot of θ as a function of α and β . It can be seen that only certain combinations of (α, β) can lead to folding. For example, when $\alpha + \beta = \pi$, folding of the crease does not change the PS sector angle. The PS sector angle is constrained by the origami pattern. No angular defect is generated and no folding occurs.

From the contour plot, the maximum dihedral angle ($\theta = \pi/3$) can be obtained at $\alpha = \pi, \beta = \pi/2$. The dihedral angle is symmetric with respect to β at $\alpha = \pi$. The accessible dihedral angle can be fully captured by changing β on $(0, \pi/2)$ while keeping $\alpha = \pi$. Figure 2C shows the experimental results of four dihedral angles between $\beta = \pi/4$ and $\beta = \pi/2$, with $\alpha = \pi$. Figure 2D plots θ as a function β of at $\alpha = \pi$. The experimental results and the analytical solution agree reasonably well. The slight deviation might be attributed to the finite stiffness of the crease (neglected in this work), which depends on the relative orientation between the crease and the angular shrinkage gadget (i.e., angle β).

For those creases that can be folded independently, one crease corresponds to one degree of freedom and can be deterministically folded by one gadget. Thus, multiple creases could be deterministically folded when gadgets of equal number are used. **Figure 3A** shows the schematic representation of folding truncated pyramids. Truncated triangular pyramid was used as an example. Around each vertex, there are three rigid paperboard sectors (in red) and one PS sector (in blue).

Shrinkage of the PS sector creates an angular defect ($2\alpha/3$) at each vertex. A cone is then formed, accompanied by folding of the paperboard sectors along the creases. The whole structure is folded in a deterministic manner. Due to symmetry of the structure, all creases are folded to the same dihedral angle.

The paperboard sector angle β_1 is equal to the interior angle of the base, which can only take discrete values

$$\beta_1 = \pi - 2\pi/n \quad (2)$$

where n is the number of sides of the base (e.g., $n = 3, 4, 5, 6$ as shown in Figure 3). The other two paperboard sectors are identical, whose angle can be calculated by subtracting β_1 and α from 2π , i.e.

$$\beta_2 = (2\pi - \alpha - \beta_1)/2 \quad (3)$$

Folding angle is defined as the dihedral angle (θ) between the lateral surface and the base of the folded structure (a truncated pyramid). Again, around each vertex, the angular defect ($2\alpha/3$) is related to the dihedral angle (θ). The calculation can be found in Figure S3 in the Supporting Information. θ as a function of α is plotted in Figure 3B. The dihedral angle θ decreases with increasing α , indicating that the bigger the angular defect, the higher the degree of folding. With the same angular defect, dihedral angles are different for different truncated pyramids.

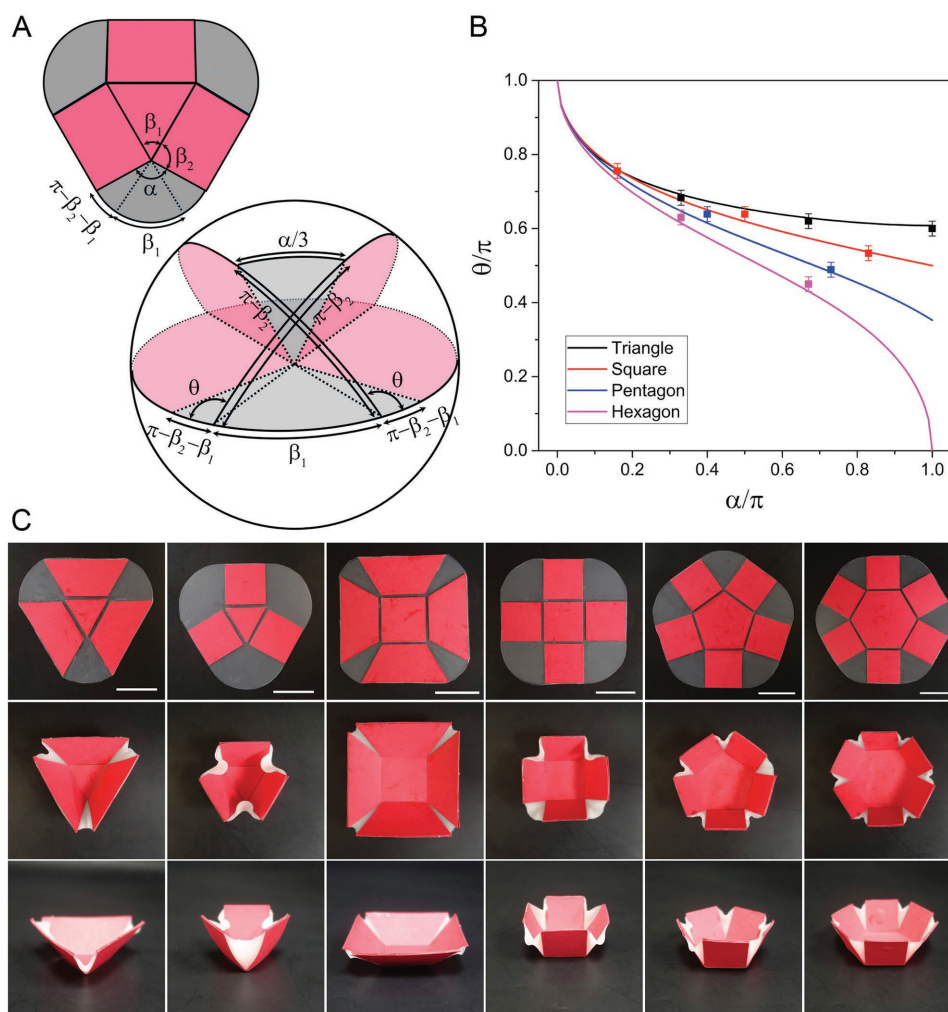


Figure 3. Folding of multiple creases using multiple angular shrinkage gadgets. A) Schematic representation of the folding and related parameters. B) Plot of the dihedral angle (θ) as a function of the sector angle (α). Four base shapes (triangle, square, pentagon, and hexagon) are shown. C) Images showing the folding of multiple creases with different base shapes (two triangles, two squares, one pentagon, and one hexagon). Top: before folding; middle: after folding (top view); bottom: after folding (perspective view). Scale bars: 30 mm.

The dihedral angle increases in the order of hexagon, pentagon, square, and triangle as the base. Figure 3C shows the optical images of truncated pyramids with different bases and different angular defects.

Another way to harness the angular shrinkage gadget is shown in Figure 4. Around the central vertex there are alternated PS sectors and paperboard sectors. Again, shrinkage of the PS sectors generates an angular defect around the vertex, transforming the flat disk into a cone. The paperboard sectors remain flat, while the PS sectors are curved. The angular defect is determined by the total angle of the PS sectors. A larger angular defect leads to a sharper cone.

2.2. Folding Using Minimal Surface Gadget

By now, we have demonstrated two ways in which a flat composite sheet can be morphed into a surface with positive Gaussian curvature by creating angular defect. A common

feature in both ways is that shrinkage occurs in the peripheral areas, while the central area is constrained. A natural question would be how the shape changes under the opposite condition, i.e., the center shrinks while the periphery is constrained. A closely related scenario is a constrained center with an expanding periphery. In that case, the periphery is wrinkled, generating a saddle surface (negative Gaussian curvature).^[12c,20] Here, we propose an alternative approach—a shrinking center with constrained periphery—and hypothesize that the sheet is morphed to a saddle surface.

Figure 5 shows the shape morphing of a PS square sheet, whose four edges were constrained by four rigid bars. The four edges cannot shrink or bend. However, the PS still tended to shrink upon heating. This can only be accommodated by rotation of the four edges and shrinkage of the angle at the four corners. Both experimental and FEA results after the shrinking are shown, which agree very well. Due to symmetry of the structure, the four corner angles shrank to the same value. The bounded PS sheet was morphed into a saddle surface

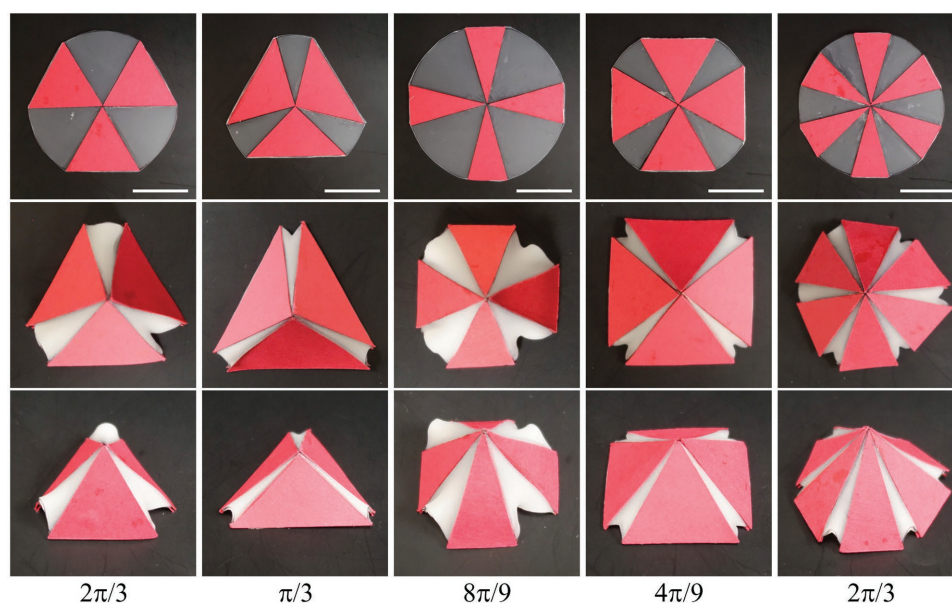


Figure 4. Folding of cones using multiple angular shrinkage gadgets. Top: before folding; middle: after folding (top view); bottom: after folding (perspective view). Angular defect of each folded cone is shown below the optical images. Scale bars: 30 mm.

(minimal surface). The structure is denoted as a minimal surface gadget. Note that two diagonals of the square shrink to about 37% of its initial length.

The minimal surface gadget can fold four edges simultaneously, which enables folding of origami loops surrounding it. **Figure 6** shows the folding of three different origami loops (square, rhombic, and square twist) and their tessellations. The structures were inspired by the kirigami pattern developed by Sussman et al.^[17c] In the center, there was a PS square or rhombic, which was surrounded by eight paperboard panels, arranged into a loop with eight creases. The four sides of the PS panel were effectively constrained by four rigid paperboard panels, making a minimal surface gadget. Upon heating, the gadget folded the origami loop into a step structure. Column B shows top view of the folded structures. For a single origami loop, there are two degenerate folded states, which are schematically illustrated in column B. One pair of opposite corners pops up, while the other pair pops down. The two degenerate configurations are symmetrically equivalent to each other, i.e., one configuration can be

converted to the other via symmetric operation. For square and square twist, one configuration can be converted to the other by 90° rotation. For rhombic, a reflection through the flat surface (mirror plane) can convert one state to the other.

The tessellations are shown below the corresponding origami loops. It can be seen that each loop had four neighbors surrounding it, each of which shared a side (three paperboard panels) with it. Adjacent origami loops are folded into different configurations, as required by the shared side. Once the folded configuration of one origami loop is given, the configurations of the other four adjacent loops can also be determined. Upon heating, all origami loops were folded in a parallel manner. A 2D pattern was thus transformed into a 3D checkerboard pattern.

In both the angular shrinkage gadget and the minimal surface gadget, biaxial shrinkage of an otherwise unconstrained, heat shrinkable polymer sheet is converted to angular shrinkage under predefined constraints, which is harnessed to fold origami structures. In the case of the angular shrinkage gadget, shrinkage is allowed in the circumferential direction,

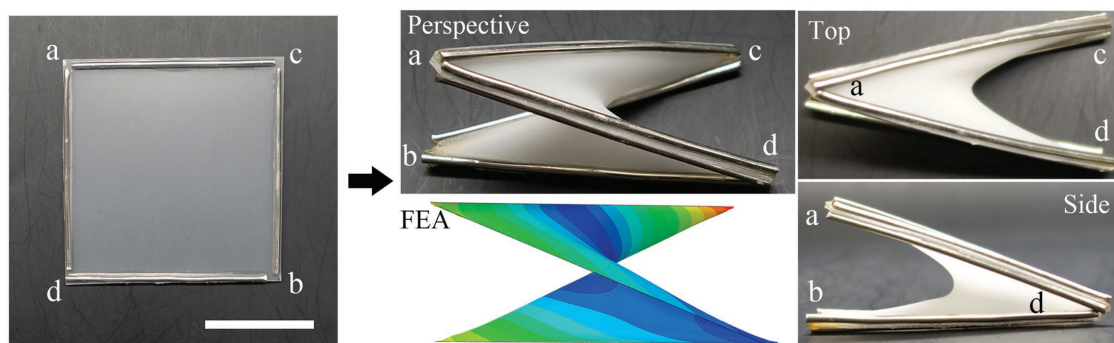


Figure 5. Minimal surface gadget. Perspective, top and side view images of the folded structure are shown. Perspective view of the FEA result is included for comparison. Scale bar: 30 mm.

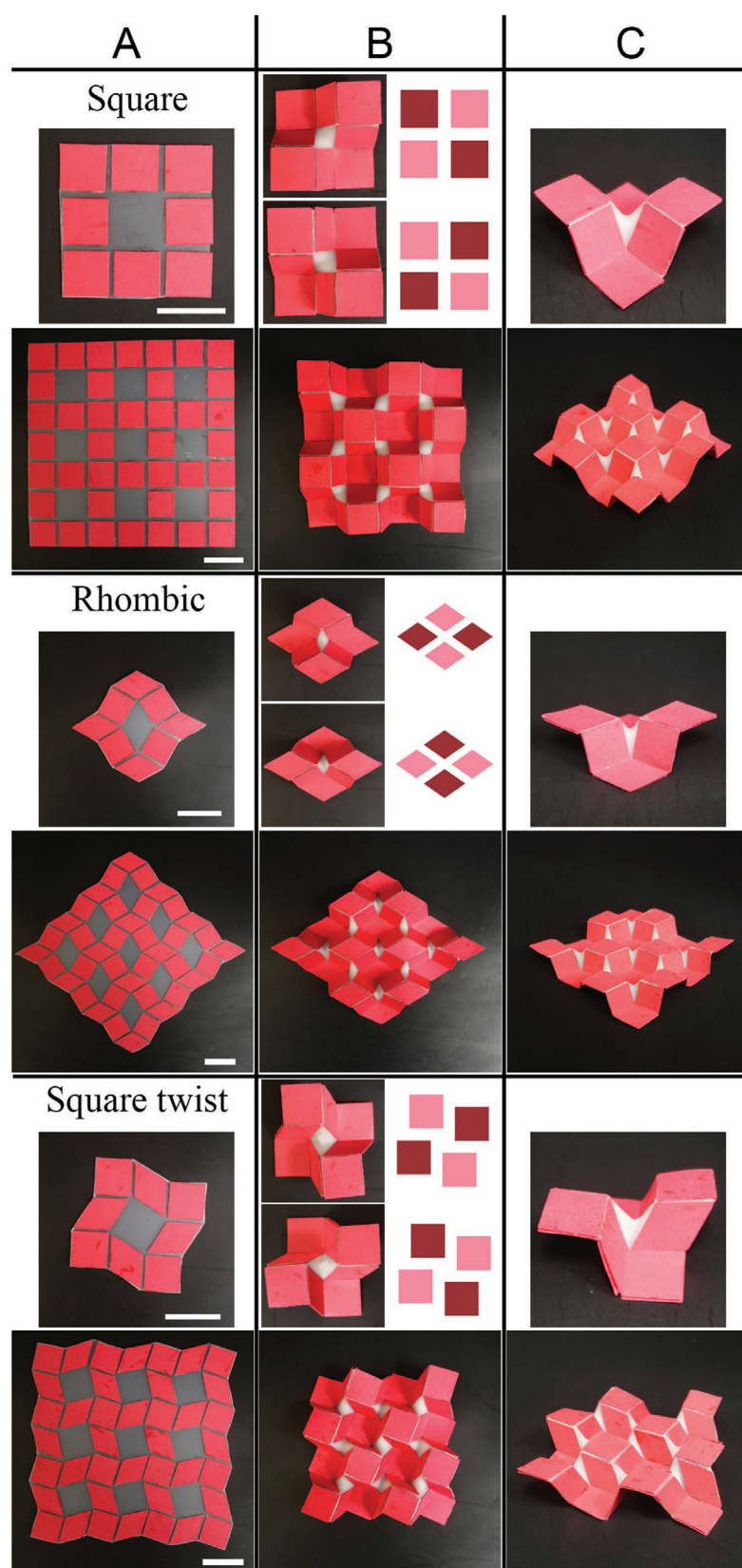


Figure 6. Folding of origami loops using minimal surface gadgets. Three different origami loops and their tessellations (below the corresponding loop) are shown. A) Flat state.

but constrained in the radial direction. More specifically, in the radial direction, the two edges are totally constrained and as a result the sector in between is partially constrained. In the case of the minimal surface gadget, where four angles shrink simultaneously, shrinkage is still allowed in the circumferential direction as in the case of the angular shrinkage gadget. But shrinkage is further constrained in the radial direction in the sectors between the four edges due to symmetry, which leads to shrinkage along both diagonals.

3. Conclusion

We have demonstrated a new approach to fold origami/kirigami structures, based on Gaussian curvature change induced by laterally nonuniform shrinkage. Flat origami/kirigami patterns were embedded into a heat shrinkable polymer sheet, making a composite sheet. The composite sheet experienced laterally nonuniform shrinkage upon heating, which changed the Gaussian curvature of the sheet and transformed the flat sheet into a 3D curved structure. The shape morphing was guided by the origami/kirigami patterns. Depending on the position of origami/kirigami patterns, curved surfaces with positive or negative Gaussian curvature can be obtained. When the origami/kirigami patterns were placed in the central area, shrinkage of the polymer sheet in the peripheral area can create 3D surfaces with positive Gaussian curvature. Examples included cones and truncated pyramids. On the other hand, when the polymer sheet was surrounded by an origami loop, saddle surfaces (with negative Gaussian curvature) can be obtained. The flat origami loop was folded into a step structure. Furthermore, tessellation of the origami loops was transformed into a 3D checkerboard pattern. This work represents a new approach to morph sheet structures, taking advantage of both shape morphing in soft materials and origami folding in rigid structures. The design approach can be applied to other responsive or active materials as long as the biaxial shrinkage is constrained with the patterns demonstrated in this work.

4. Experimental Section

Sample Preparation and Folding Experiments: The heat shrinkable polymer sheet was made of prestrained PS (Grafix Shrink Film) with the thickness of 0.25 mm. The

B) Top view of the folded state. C) Perspective view of the folded state. Each origami loop can be folded into two degenerate states, which is schematically shown on the right side of column (B). Bright color indicates pop-up while dark color indicates pop-down. Scale bars: 30 mm.

PS sheet shrunk in-plane equibiaxially to 50% of initial dimensions upon heating ($\approx 150^\circ\text{C}$). The rigid bars used for constraining PS sheet were metal wires (glued on the edges of the PS sheet). The origami patterns were fabricated by gluing paperboard panels (cut from Staples file folder) on selected areas of the PS sheet. The paperboard panels were glued on both sides of the PS sheet using superglue (Loctite Liquid Professional Super Glue 20-Gram Bottle). A gap was left between adjacent panels to define the crease. The areas glued with paperboard panels cannot deform. After the glue was fully cured, samples were put in the oven for folding.

Finite Element Simulation: 3D FEA of the folding of PS sheets was carried out in Abaqus 6.14. The radial structures with an initial angle ranging from 30° to 180° were modeled with a radius of 30 mm and thickness of 0.25 mm, in accordance with the experiments (Figure 1). Both straight sides were constrained via the multipoint constrain method throughout the simulations. The square structure was modeled with a side length of 60 mm and thickness of 0.25 mm (Figure 5). Similar to the previous case, all sides were constrained. Four-node curved shell with reduced integration elements (S4R) was used to model PS. Isotropic linear elastic behavior was assumed with Young's modulus of 3 GPa and Poisson's ratio of 0.4. A thermal strain of -0.5 was set, while a small perturbation force was applied at the center of both structures in order to trigger out-of-plane buckling.

Supporting Information

Supporting Information is available from the Wiley Online Library or from the author.

Acknowledgements

This work was supported by the NSF under the Emerging Frontiers in Research and Innovation program (Award No. EFRI-1240438).

Conflict of Interest

The authors declare no conflict of interest.

Keywords

Gaussian curvature, heat shrinkable polymers, origami/kirigami, shape morphing

Received: April 23, 2018
Revised: June 24, 2018
Published online: August 1, 2018

- [1] a) M. Zarek, M. Layani, I. Cooperstein, E. Sachyani, D. Cohn, S. Magdassi, *Adv. Mater.* **2016**, *28*, 4449; b) S. Xu, Z. Yan, K.-I. Jang, W. Huang, H. Fu, J. Kim, Z. Wei, M. Flavin, J. McCracken, R. Wang, A. Badea, Y. Liu, D. Xiao, G. Zhou, J. Lee, H. U. Chung, H. Cheng, W. Ren, A. Banks, X. Li, U. Paik, R. G. Nuzzo, Y. Huang, Y. Zhang, J. A. Rogers, *Science* **2015**, *347*, 154; c) Z. Song, T. Ma, R. Tang, Q. Cheng, X. Wang, D. Krishnaraju, R. Panat, C. K. Chan, H. Yu, H. Jiang, *Nat. Commun.* **2014**, *5*, 3140.
- [2] a) R. F. Shepherd, F. Ilievski, W. Choi, S. A. Morin, A. A. Stokes, A. D. Mazzeo, X. Chen, M. Wang, G. M. Whitesides, *Proc. Natl. Acad. Sci. USA* **2011**, *108*, 20400; b) S. Felton, M. Tolley, E. Demaine, D. Rus, R. Wood, *Science* **2014**, *345*, 644; c) F. Ilievski, A. D. Mazzeo, R. F. Shepherd, X. Chen, G. M. Whitesides, *Angew. Chem.* **2011**, *123*, 1930.
- [3] a) M. W. Han, S. H. Ahn, *Adv. Mater.* **2017**, *29*, 1606580; b) J. Hu, H. Meng, G. Li, S. I. Ibekwe, *Smart Mater. Struct.* **2012**, *21*, 053001.
- [4] a) R. Fernandes, D. H. Gracias, *Adv. Drug Delivery Rev.* **2012**, *64*, 1579; b) J. Guan, H. He, L. J. Lee, D. J. Hansford, *Small* **2007**, *3*, 412.
- [5] a) Y. Liu, J. Genzer, M. D. Dickey, *Prog. Polym. Sci.* **2016**, *52*, 79; b) S.-J. Jeon, A. W. Hauser, R. C. Hayward, *Acc. Chem. Res.* **2017**, *50*, 161; c) Y. Zhang, F. Zhang, Z. Yan, Q. Ma, X. Li, Y. Huang, J. A. Rogers, *Nat. Rev. Mater.* **2017**, *2*, 17019.
- [6] a) P. Froeter, X. Yu, W. Huang, F. Du, M. Li, I. Chun, S. H. Kim, K. J. Hsia, J. A. Rogers, X. Li, *Nanotechnology* **2013**, *24*, 475301; b) A. S. Gladman, E. A. Matsumoto, R. G. Nuzzo, L. Mahadevan, J. A. Lewis, *Nat. Mater.* **2016**, *15*, 413.
- [7] a) Y. Liu, B. Shaw, M. D. Dickey, J. Genzer, *Sci. Adv.* **2017**, *3*, e1602417; b) Q. Zhang, J. Wommer, C. O'Rourke, J. Teitelman, Y. Tang, J. Robison, G. Lin, J. Yin, *Extreme Mech. Lett.* **2017**, *11*, 111; c) J. Cui, S. Yao, Q. Huang, J. G. Adams, Y. Zhu, *Soft Matter* **2017**, *13*, 3863.
- [8] M. Lee, S. Kim, H.-Y. Kim, L. Mahadevan, *Phys. Fluids* **2016**, *28*, 042101.
- [9] a) J. H. Na, A. A. Evans, J. Bae, M. C. Chiappelli, C. D. Santangelo, R. J. Lang, T. C. Hull, R. C. Hayward, *Adv. Mater.* **2015**, *27*, 79; b) J. Jeong, Y. Cho, S. Y. Lee, X. Gong, R. D. Kamien, S. Yang, A. Yodh, *Soft Matter* **2017**, *13*, 956; c) E. Smela, O. Innganas, I. Lundstrom, *Science* **1995**, *268*, 1735; d) L. Zhang, E. Deckhardt, A. Weber, C. Schönenberger, D. Grützmacher, *Nanotechnology* **2005**, *16*, 655; e) M. T. Tolley, S. M. Felton, S. Miyashita, D. Aukes, D. Rus, R. J. Wood, *Smart Mater. Struct.* **2014**, *23*, 094006; f) S. Yao, J. Cui, Z. Cui, Y. Zhu, *Nanoscale* **2017**, *9*, 3797; g) S. Miyashita, S. Guitron, M. Lüdgersdorfer, C. R. Sung, D. Rus, presented at *2015 IEEE Int. Conf. on Robotics and Automation (ICRA)*, Seattle, WA, USA **2015**.
- [10] M. Finot, S. Suresh, *J. Mechanics Phys. Solids* **1996**, *44*, 683.
- [11] a) Y. Zhang, Z. Yan, K. Nan, D. Xiao, Y. Liu, H. Luan, H. Fu, X. Wang, Q. Yang, J. Wang, W. Ren, H. Si, F. Liu, L. Yang, H. Li, J. Wang, X. Guo, H. Luo, L. Wang, Y. Huang, J. A. Rogers, *Proc. Natl. Acad. Sci. USA* **2015**, *112*, 11757; b) J. Cui, J. Adams, Y. Zhu, *Smart Mater. Struct.* **2017**, *26*, 125011.
- [12] a) J. Kim, J. A. Hanna, M. Byun, C. D. Santangelo, R. C. Hayward, *Science* **2012**, *335*, 1201; b) A. M. Hubbard, R. W. Mailen, M. A. Zikry, M. D. Dickey, J. Genzer, *Soft Matter* **2017**, *13*, 2299; c) Y. Klein, E. Efrati, E. Sharon, *Science* **2007**, *315*, 1116.
- [13] Z. L. Wu, M. Moshe, J. Greener, H. Therien-Aubin, Z. Nie, E. Sharon, E. Kumacheva, *Nat. Commun.* **2013**, *4*, 1586.
- [14] S. Tibbits, *Archit. Des.* **2012**, *82*, 68.
- [15] a) R. J. Lang, presented at *Proc. of the Twelfth Annual Symp. on Computational Geometry*, Philadelphia, Pennsylvania, USA **1996**; b) T. Tachi, presented at *The Fourth Int. Conf. on Origami in Science, Mathematics, and Education* (Ed.: R. Lang), CRC Press, Boca Raton, Florida, USA **2009**.
- [16] a) D. A. Huffman, *IEEE Trans. Comput.* **1976**, *25*, 1010; b) L. H. Dudte, E. Vouga, T. Tachi, L. Mahadevan, *Nat. Mater.* **2016**, *15*, 583; c) S. J. Callens, A. A. Zadpoor, *Mater. Today* **2017**, *21*, 241.
- [17] a) T. Castle, Y. Cho, X. Gong, E. Jung, D. M. Sussman, S. Yang, R. D. Kamien, *Phys. Rev. Lett.* **2014**, *113*, 245502; b) Y. Tang, G. Lin, S. Yang, Y. K. Yi, R. D. Kamien, J. Yin, *Adv. Mater.* **2017**, *29*; c) D. M. Sussman, Y. Cho, T. Castle, X. Gong, E. Jung, S. Yang, R. D. Kamien, *Proc. Natl. Acad. Sci. USA* **2015**, *112*, 7449; d) F. Wang, X. Guo, J. Xu, Y. Zhang, C. Chen, *J. Appl. Mech.* **2017**, *84*, 061007.
- [18] E. A. Peraza-Hernandez, D. J. Hartl, R. J. Malak Jr., D. C. Lagoudas, *Smart Mater. Struct.* **2014**, *23*, 094001.
- [19] E. D. Demaine, J. O'Rourke, *Geometric Folding Algorithms*, Cambridge University Press, Cambridge **2007**.
- [20] a) C. Huang, D. Quinn, S. Suresh, K. J. Hsia, *Proc. Natl. Acad. Sci. USA* **2017**, 201717912; b) T. Mora, A. Boudaoud, *Eur. Phys. J. E* **2006**, *20*, 119.